

Phase Structure and Electrochemical Properties of $\text{La}_{0.7}\text{Ce}_{0.3}\text{Ni}_{3.83-x}\text{Mn}_{0.43}\text{Co}_{0.25}\text{Al}_{0.26}\text{Cu}_{0.48}(\text{Fe}_{0.43}\text{B}_{0.57})_x$ Hydrogen Storage Alloys

Youchao Wang¹, Yanping Fan², Anming Li^{1,*}

¹ School of Materials Science & Engineering, Henan Polytechnic University, Jiaozuo 454000, China

² School of Physics and Chemistry, Henan Polytechnic University, Jiaozuo 454000, China

*E-mail: hpuforrest@126.com

Received: 26 February 2013 / Accepted: 22 March 2013 / Published: 1 April 2013

Microstructures and electrochemical characteristics of $\text{La}_{0.7}\text{Ce}_{0.3}\text{Ni}_{3.83-x}\text{Mn}_{0.43}\text{Co}_{0.25}\text{Al}_{0.26}\text{Cu}_{0.48}(\text{Fe}_{0.43}\text{B}_{0.57})_x$ hydrogen storage alloys have been investigated. X-ray diffraction results indicate that the pristine alloy is single LaNi_5 phase with CaCu_5 type hexagonal structure and the alloys containing $\text{Fe}_{0.43}\text{B}_{0.57}$ consist of two phases, LaNi_5 matrix phase and $\text{La}_3\text{Ni}_{13}\text{B}_2$ secondary phase. The abundance of $\text{La}_3\text{Ni}_{13}\text{B}_2$ phase increases with the increase of x value. The substitution of Ni by $\text{Fe}_{0.43}\text{B}_{0.57}$ contributes to the activation property of alloy electrodes. Maximum discharge capacity of the alloy electrodes monotonically decreases from 302.5 mAh/g ($x = 0$) mAh/g to 277.1 ($x = 0.20$) with increasing x value. High-rate dischargeability of the alloy electrodes first increases with increasing x from 0 to 0.15, and then decreases until x increases to 0.20. Cycling stability decreases with increasing x from 0 to 0.20. The adequate substitution of Ni by FeB can improve the overall electrochemical performances and reduce the raw cost of alloy electrode.

Keywords: Hydrogen storage alloy; Phase structure; Electrochemical property; Ni/MH batteries; Co-less alloy

1. INTRODUCTION

AB_5 -type (Original LaNi_5) hydrogen storage alloys are widely used as the negative electrode materials in commercial nickel/metal hydride (Ni-MH) batteries [¹]. However, wide applications of Ni-MH battery are hindered due to the high cost of negative electrode materials. Co-less or Co-free alloys

were developed by substituting Co or Ni by cheap metals, such as, Fe, Cu and Si, etc. [2-4]. $\text{La}_{0.7}\text{Ce}_{0.3}\text{Ni}_{3.83}\text{Mn}_{0.43}\text{Co}_{0.25}\text{Al}_{0.26}\text{Cu}_{0.48}$ alloy was developed and commercially produced [5]. However, the electrochemical performance of the alloy is still not satisfying. Thus, it is necessary to further improve electrochemical hydrogen storage properties without increasing raw cost of the Co-less alloys.

Ye et al. [6] reported that the addition of boron significantly improved the high-rate capacity and modified the activation performance of $\text{Mm}_{3.55}\text{Co}_{0.75}\text{Mn}_{0.4}\text{Al}_{0.3}\text{B}_x$ alloy though the electrochemical capacity was lower than that of commercial $\text{Mm}_{3.55}\text{Co}_{0.75}\text{Mn}_{0.4}\text{Al}_{0.3}$ alloy. Zhang et al. [7] studied hydrogen storage properties of $\text{MmNi}_{3.8}\text{Co}_{0.4}\text{Mn}_{0.6}\text{Al}_{0.2}\text{B}_x$ alloys and pointed out that the addition of B enhanced the cycling stability, activation performance and high-rate discharge capability. Yang et al. [8] found that the substitution of B for Ni in $\text{MmNi}_{3.70-x}\text{Mn}_{0.35}\text{Co}_{0.60}\text{Al}_{0.25}\text{B}_x$ hydrogen storage alloys improved the activation ability and the high-rate dischargeability of the alloy electrodes. The addition of B element has been proved to be effective to enhance the activation performance and the high-rate dischargeability. Therefore, it can be expected that the high-rate dischargeability and activation property could be improved by substituting B for Ni in the AB_5 -type hydrogen storage alloys. However, the pure B is very expensive and unpractical to be used in the Co-less alloy. Fortunately, the cost of commercial $\text{Fe}_{0.43}\text{B}_{0.57}$ alloy is obviously lower than that of pure B, and the $\text{Fe}_{0.43}\text{B}_{0.57}$ alloy has much lower melt point than that of pure B, and then facilitates the homogeneity of the alloy. In addition, Liu et al. [9-12] have reported that $\text{Fe}_{0.43}\text{B}_{0.57}$ can replace B as additive in Co-less or Co-free alloy. Thus, it is feasible and promising to substitute Ni using $\text{Fe}_{0.43}\text{B}_{0.57}$ in Co-less AB_5 -type alloy.

In this work, on the basis of the merits of $\text{Fe}_{0.43}\text{B}_{0.57}$ alloy and the belief that the Fe and B addition may result in some noticeable modification of the electrochemical properties, microstructures and electrochemical hydrogen storage properties of $\text{La}_{0.7}\text{Ce}_{0.3}\text{Ni}_{3.83-x}\text{Mn}_{0.43}\text{Co}_{0.25}\text{Al}_{0.26}\text{Cu}_{0.48}(\text{Fe}_{0.43}\text{B}_{0.57})_x$ ($x = 0-0.20$) alloys have been investigated.

2. EXPERIMENTAL PROCEDURES

$\text{La}_{0.7}\text{Ce}_{0.3}\text{Ni}_{3.83-x}\text{Mn}_{0.43}\text{Co}_{0.25}\text{Al}_{0.26}\text{Cu}_{0.48}(\text{Fe}_{0.43}\text{B}_{0.57})_x$ ($x = 0-0.20$) alloys were synthesized by induction melting of the metal elements (La, Ce, Ni, Mn, Al, Cu: 99.9% purity, $\text{Fe}_{0.43}\text{B}_{0.57}$ alloy contained 57.0 at.% B and the other were Fe and trace impurities) in Ar atmosphere, and then were annealed at 1273 K for 10 h in Ar atmosphere with the pressure of 0.08 MPa.

The phases of the alloy powders were determined by X-ray diffraction (XRD) using a Rigaku D/max 2500PC powder diffractometer with Cu $K\alpha$ radiation. The phase structure of the alloys was analyzed using Jade-5 software.

The alloy powders of measuring electrodes were obtained by grinding the inner part of alloy ingots in the Ar atmosphere. All measuring electrodes were prepared by cold pressing the mixture of 0.15 g alloy powders of 200-400 meshes and 0.75 g nickel carbonyl powders into a pellet of 10 mm in diameter under 15 MPa. Electrochemical measurements were performed at 298 K in a standard tri-

electrode system, consisting of a working electrode (metal hydride), a counter electrode ($\text{Ni}(\text{OH})_2/\text{NiOOH}$), and a reference electrode (Hg/HgO) with 6mol/L KOH solution as electrolyte. Each electrode was charged for 7 h at 60 mA/g and discharged to -0.6 V versus Hg/HgO at 60 mA/g at 298 K. After every charging/discharging, the rest time was 10 min. In evaluating the high-rate dischargeability, discharge capacity of the alloy electrode at different discharge current density were measured. The high-rate dischargeability HRD (%) was defined as $C_d/C_{\max} \times 100\%$, where C_d was the discharge capacity at the discharge current density I_d ($I_d = 60, 300, 600, 900$ and 1200 mA/g) and C_{\max} was the maximum discharge capacity at the discharge current density $I = 60$ mA/g.

The electrochemical impedance spectrum (EIS), the linear polarization curve and potential-step measurement were obtained by on PARSTAT 2273, respectively. At 50% depth of discharge (DOD), linear polarization curve was obtained by scanning the electrodes from -5 to 5 mV (vs. open circuit potential) at 50% DOD. For potential-step measurement, the electrodes in fully charged state were discharged with potential steps of 0.5 V for 3600 s.

3. RESULTS AND DISCUSSION

3.1 Crystal structure

Fig. 1 shows XRD patterns of $\text{La}_{0.7}\text{Ce}_{0.3}\text{Ni}_{3.83-x}\text{Mn}_{0.43}\text{Co}_{0.25}\text{Al}_{0.26}\text{Cu}_{0.48}(\text{Fe}_{0.43}\text{B}_{0.57})_x$ alloys. It can be seen that $\text{La}_{0.7}\text{Ce}_{0.3}\text{Ni}_{3.83}\text{Mn}_{0.43}\text{Co}_{0.25}\text{Al}_{0.26}\text{Cu}_{0.48}$ alloy is single LaNi_5 phase with CaCu_5 structure, and the alloys containing $\text{Fe}_{0.43}\text{B}_{0.57}$ consist of two phases, LaNi_5 matrix phase and $\text{La}_3\text{Ni}_{13}\text{B}_2$ secondary phase. The abundance of $\text{La}_3\text{Ni}_{13}\text{B}_2$ phase increases with the increase of x value.

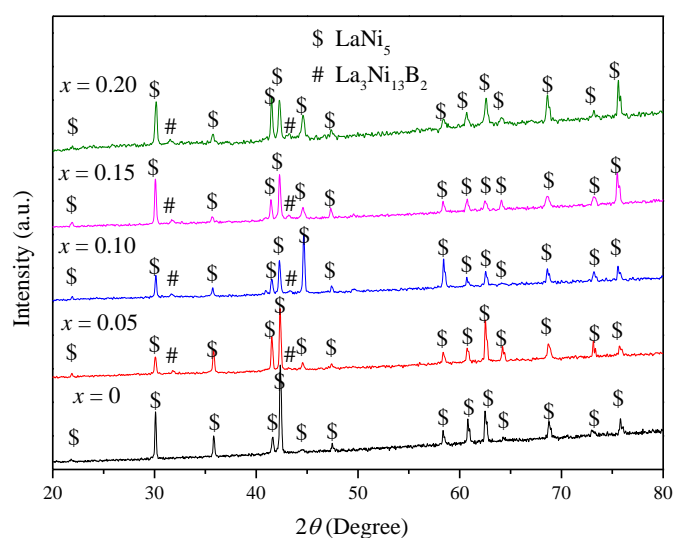


Figure 1. XRD patterns of $\text{La}_{0.7}\text{Ce}_{0.3}\text{Ni}_{3.83-x}\text{Mn}_{0.43}\text{Co}_{0.25}\text{Al}_{0.26}\text{Cu}_{0.48}(\text{Fe}_{0.43}\text{B}_{0.57})_x$ alloys

3.2 Activation capability and discharge capability

The number of cycles (N_a) needed to activate the electrodes and maximum discharge capacity (C_{max}) of $\text{La}_{0.7}\text{Ce}_{0.3}\text{Ni}_{3.83-x}\text{Mn}_{0.43}\text{Co}_{0.25}\text{Al}_{0.26}\text{Cu}_{0.48}(\text{Fe}_{0.43}\text{B}_{0.57})_x$ alloy electrodes are given in Table 1. It is noted that N_a decreases from 7 ($x = 0$) to 2 ($x = 0.20$) with increasing x value, indicating the substitution of Ni by $\text{Fe}_{0.43}\text{B}_{0.57}$ contributes to the activation properties of alloy electrode. Shu et al. [13] and Zhang et al. [14] pointed out that the phase interface or grain boundary contributes to the activation of alloy electrode because the interface or boundary was a buffer area of the releasing of the lattice stress and strain energy. According to the XRD results, the phase interface increases with increasing x values, which is beneficial to the activation properties. Moreover, B can effectively improve the surface electrochemical activity of alloy surface [8]. The increase of B contributes to the electrochemical activity of alloy surface, and therefore increases the activation property. However, it is believed that the metallic Ni in the alloy surface acts as an electrocatalyst for the rapid activation [15-17]. Ni content on the alloy surface decreases with increasing x value, which is detrimental to the activation properties. Consequently, the advantageous factor is prominent for the improvement in the activation property of the alloy electrodes in present work. The C_{max} of the alloy electrodes decreases from 302.5 mAh/g ($x = 0$) mAh/g to 277.1 ($x = 0.20$) with increasing x value, which should be ascribed to the following factors. Firstly, the hydrogen storage capacity of $\text{La}_3\text{Ni}_{13}\text{B}_2$ phase is 157 mAh/g [18], which is much lower than that of the matrix CaCu_5 -type phase. The $\text{La}_3\text{Ni}_{13}\text{B}_2$ phase increases gradually with increasing amount of $\text{Fe}_{0.43}\text{B}_{0.57}$, which is unfavorable for the discharge capacity. Secondly, the increase in Fe content leads to the increase in surface oxide film, which degrades the charge-transfer reaction. The surface oxide film decreases the activity site on the alloy surface, and then makes the hydrogen diffuse from the inner of alloy to the surface more difficult. Thirdly, Ni is beneficial to the charge-transfer reaction at the electrode/electrolyte interface due to excellent electrocatalytic activity and makes the hydrogen diffusion through the surface more easily due to good electrical conductivity [19]. As x increases, the decrease in Ni content with increasing x value degrades the charge-transfer reaction and hydrogen diffusion, and then lead to a decrease in the discharge capacity.

Table 1. Electrochemical properties of $\text{La}_{0.7}\text{Ce}_{0.3}\text{Ni}_{3.83-x}\text{Mn}_{0.43}\text{Co}_{0.25}\text{Al}_{0.26}\text{Cu}_{0.48}(\text{Fe}_{0.43}\text{B}_{0.57})_x$ alloy electrodes

x	C_{max} (mAh/g)	N_a	HRD ₁₂₀₀ ^a (%)	S_{100} (%)
0	302.5	7	48.9	94.2
0.05	298.4	6	53.9	90.2
0.10	292.3	4	60.5	88.5
0.15	281.2	3	65.8	86.1
0.20	277.1	2	63.3	84.3

^a The high-rate dischargeability at the discharge current density of 1200 mA/g.

3.3 High rate dischargeability and electrochemical kinetics

Fig. 2 shows the relationship between the high-rate dischargeability (HRD) and the discharge current density of $\text{La}_{0.7}\text{Ce}_{0.3}\text{Ni}_{3.75-x}\text{Cu}_{0.75}\text{Mn}_{0.35}\text{Al}_{0.15}(\text{Fe}_{0.43}\text{B}_{0.57})_x$ alloy electrodes. The HRD of the alloy electrodes first increases with increasing x from 0 to 0.15, and then decreases until x increases to 0.20. The HRD at the discharge current density of 1200 mA/g (HRD_{1200}) is listed in Table 1. It can be seen that HRD_{1200} first increases from 48.9% ($x = 0$) to 65.8% ($x = 0.15$), and then decreases to 63.3% ($x = 0.20$).

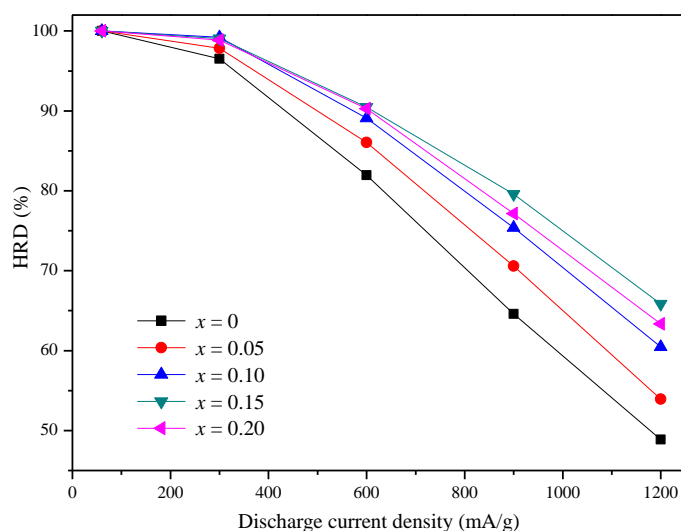


Figure 2. HRD of $\text{La}_{0.7}\text{Ce}_{0.3}\text{Ni}_{3.83-x}\text{Mn}_{0.43}\text{Co}_{0.25}\text{Al}_{0.26}\text{Cu}_{0.48}(\text{Fe}_{0.43}\text{B}_{0.57})_x$ alloy electrodes

It is well known that the HRD of the metal hydride electrodes are influenced mainly by the charge-transfer kinetics at the electrode/electrolyte interface and hydrogen diffusion rate in the bulk of alloy [20]. The exchange current density I_0 of alloy electrode is commonly used to characterize the catalytic activity for charge-transfer reaction at the electrode/electrolyte interface, and limited current density (I_L) is used to characterize hydrogen diffusion rate in the bulk of alloy.

The I_0 determined from linear micropolarization curve is the rate of hydriding/dehydriding at the equilibrium state and can be used to evaluate electrocatalytic activity for charge-transfer reaction on the surface of alloy electrodes. Fig. 3 shows the linear polarization curves of $\text{La}_{0.7}\text{Ce}_{0.3}\text{Ni}_{3.83-x}\text{Mn}_{0.43}\text{Co}_{0.25}\text{Al}_{0.26}\text{Cu}_{0.48}(\text{Fe}_{0.43}\text{B}_{0.57})_x$ alloy electrodes at 50% DOD and 298 K. The polarization resistances (R_p) is calculated through estimating the slopes of linear polarization curves, and listed in Table 2. The R_p values of the alloy electrodes first decreases from 191.8 mΩ g ($x = 0$) to 143.3 mΩ g ($x = 0.15$), and then increases to 148.1 mΩ g ($x = 0.20$) with increasing x value. The I_0 value can be calculated according to the following formula [21] and listed in Table 3.

$$I_0 = \frac{RT}{FR_p} \quad (1)$$

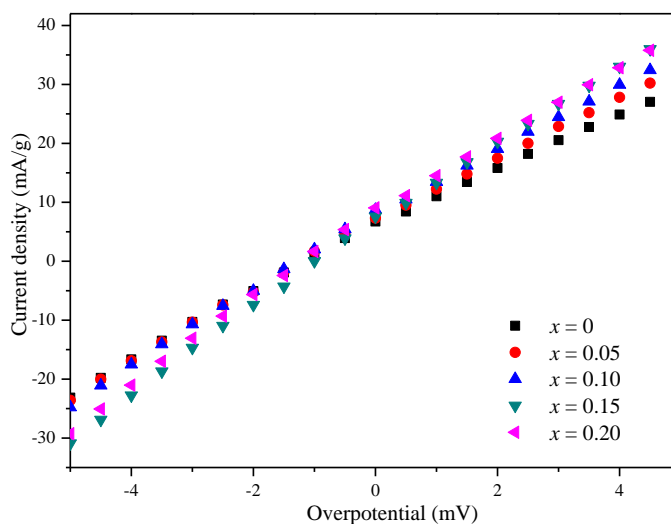


Figure 3. Linear polarization curves of $\text{La}_{0.7}\text{Ce}_{0.3}\text{Ni}_{3.83-x}\text{Mn}_{0.43}\text{Co}_{0.25}\text{Al}_{0.26}\text{Cu}_{0.48}(\text{Fe}_{0.43}\text{B}_{0.57})_x$ alloy electrodes

Table 2. Electrochemical kinetic characteristics of $\text{La}_{0.7}\text{Ce}_{0.3}\text{Ni}_{3.83-x}\text{Mn}_{0.43}\text{Co}_{0.25}\text{Al}_{0.26}\text{Cu}_{0.48}(\text{Fe}_{0.43}\text{B}_{0.57})_x$ alloy electrodes

x	R_p ($\text{m}\Omega \text{ g}$)	I_0 (mA/g)	I_L (mA/g)
0	191.8	133.9	2227.6
0.05	178.9	143.5	2429.4
0.10	168.2	152.7	2640.4
0.15	143.4	179.1	2742.5
0.20	148.1	173.4	2669.2

where R , T , F , R_p are the gas constant, absolute temperature, Faraday constant and the polarization resistance, respectively. Clearly the I_0 first increases from 133.9 mA/g ($x = 0$) to 179.1 mA/g ($x = 0.15$), and then decreases to 173.4 mA/g ($x = 0.20$). Increasing B will increase the electrochemical activity [22], which is favorable to the charge-transfer reaction of the alloy electrodes. On the other hand, as mentioned above, as x increases, the decrease in Ni content with increasing x

value degrade the charge-transfer reaction on the alloy surface. Therefore, it is certain that the exchange current density has a maximum value with increasing x value.

Fig. 4 shows the anodic polarization of $\text{La}_{0.7}\text{Ce}_{0.3}\text{Ni}_{3.83-x}\text{Mn}_{0.43}\text{Co}_{0.25}\text{Al}_{0.26}\text{Cu}_{0.48}(\text{Fe}_{0.43}\text{B}_{0.57})_x$ alloy electrodes at 50 % DOD and 298 K. It can be seen that the anodic current density increases with increasing overpotential and finally reaches a limiting value defined as the limiting current density I_L [23]. In general, the limiting current density I_L represents the hydrogen diffusivity in the bulk of the alloys, that is, the larger the I_L value, the faster is the diffusion of the hydrogen atoms in the alloys [24]. The I_L values are also summarized in Table 2. The I_L of the alloy electrodes first increases from 2227.6 mA/g ($x = 0$) to 2742.5 mA/g ($x = 0.15$), and then decreases to 2669.2 mA/g ($x = 0.20$), indicating the hydrogen diffusion performance first increases with increase x from 0 to 0.15, and then decreases until x decreases to 0.20. The formation of the secondary phase increases the fraction of phase boundaries, which provides extra tunnels for the diffusion of hydrogen atoms [13]. The increase of $\text{La}_3\text{Ni}_{13}\text{B}_2$ secondary phase causes the increase in the phase boundary, which can decrease the lattice distortion and strain energy formed in the process of hydrogen absorption. Moreover, the increase of B content with increasing x value lowers the stability of the alloy hydride [22], which contributes to the hydrogen desorption, which is beneficial to the hydrogen diffusion. Conversely, Khaldi et al. [25] have reported that the oxidation of Fe on the alloy surface limited the hydrogen transfer from the surface to the bulk. The increase in Fe content causes the increase in surface oxide film, which will degrade the hydrogen diffusion. Consequently, the threshold content of $\text{Fe}_{0.43}\text{B}_{0.57}$ is 0.15 in present system.

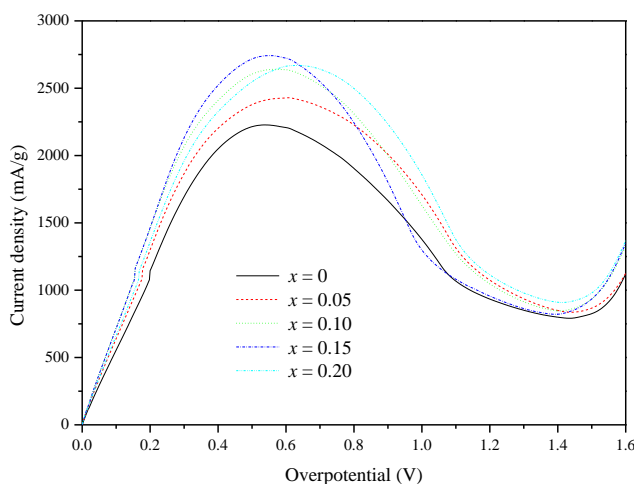


Figure 4. Anodic polarization curves of $\text{La}_{0.7}\text{Ce}_{0.3}\text{Ni}_{3.83-x}\text{Mn}_{0.43}\text{Co}_{0.25}\text{Al}_{0.26}\text{Cu}_{0.48}(\text{Fe}_{0.43}\text{B}_{0.57})_x$ alloy electrodes

3.4 Cycling stability

The cycling capacity retention rate is expressed as $S_n(\%) = C_n/C_{\max} \times 100$ (where C_n is the discharge capacity at the n th cycle). The cycling capacity retention of $\text{La}_{0.7}\text{Ce}_{0.3}\text{Ni}_{3.83-x}$

$x\text{Mn}_{0.43}\text{Co}_{0.25}\text{Al}_{0.26}\text{Cu}_{0.48}(\text{Fe}_{0.43}\text{B}_{0.57})_x$ alloy electrode as a function of cycle number is shown in Fig. 5. Cycling stability decreases with increasing x from 0 to 0.20. It can be seen from Table 1 that S_{100} decreases from 94.2% ($x = 0$) to 84.3% ($x = 0.20$). Generally, the capacity decay of the alloy electrode was ascribed to the pulverization and corrosion [26], as well as to the decrease of the electrochemical kinetics at the surface [27].

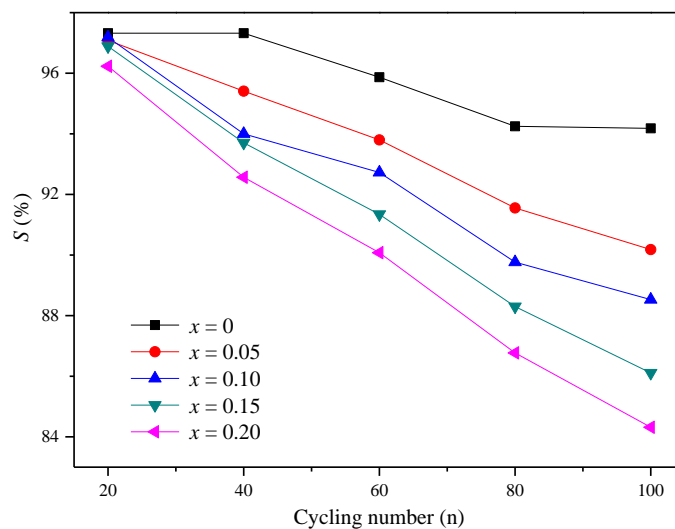


Figure 5. Cycling stability of $\text{La}_{0.7}\text{Ce}_{0.3}\text{Ni}_{3.83-x}\text{Mn}_{0.43}\text{Co}_{0.25}\text{Al}_{0.26}\text{Cu}_{0.48}(\text{Fe}_{0.43}\text{B}_{0.57})_x$ alloy electrodes

The formation of the secondary phase increases the number of phase boundary as buffer areas for the release of distortion and stress of crystal lattice in the charging/discharging process, and then restricted the pulverization [28]. The $\text{La}_3\text{Ni}_{13}\text{B}_2$ secondary phase increases the amount of phase boundary, which releases the stress formed in the process of hydrogen absorbing and then improves anti-pulverization of the alloy electrodes. However, iron corrodes more easily in the alkaline electrolyte compared with cobalt due to the lower surface energy. The increase of Fe content and decrease of Ni content will degrade the corrosion resistance of alloy electrode, and then deteriorate the cycling stability of alloy electrode. Obviously the disadvantageous factors is prominent for cycling stability of $\text{La}_{0.7}\text{Ce}_{0.3}\text{Ni}_{3.83-x}\text{Mn}_{0.43}\text{Co}_{0.25}\text{Al}_{0.26}\text{Cu}_{0.48}(\text{Fe}_{0.43}\text{B}_{0.57})_x$ alloy electrodes.

4. CONCLUSIONS

$\text{La}_{0.7}\text{Ce}_{0.3}\text{Ni}_{3.83-x}\text{Mn}_{0.43}\text{Co}_{0.25}\text{Al}_{0.26}\text{Cu}_{0.48}(\text{Fe}_{0.43}\text{B}_{0.57})_x$ ($x = 0-0.20$) alloys have been investigated. XRD results indicate that the pristine alloy has a single LaNi_5 phase, and the alloys containing $\text{Fe}_{0.43}\text{B}_{0.57}$ consist of two phases, the matrix LaNi_5 phase and the secondary phase $\text{La}_3\text{Ni}_{13}\text{B}_2$. The abundance of $\text{La}_3\text{Ni}_{13}\text{B}_2$ phase increases with the increase of x value. Maximum discharge capacity of

the alloy electrodes monotonically from 302.5 mAh/g ($x = 0$) mAh/g to 277.1 ($x = 0.20$) with increasing x value. HRD₁₂₀₀ first increases from 48.9% ($x = 0$) to 65.8% ($x = 0.15$), and then decreases to 63.3% ($x = 0.20$). S_{100} monotonically decreases from 94.2% ($x = 0$) to 84.3% ($x = 0.20$). The adequate substitution of Ni by FeB can improve the electrochemical performances and reduce the raw cost of alloy electrode.

ACKNOWLEDGEMENTS

This research is financially supported by the National Natural Science Foundation of China (51001043), China Postdoctoral Science Special Foundation (201104390), China Postdoctoral Science Foundation (20100470990), Baotou Science and Technology Project (2011J1003) and the Doctoral Foundation of Henan Polytechnic University (B2010-13).

References

1. T. Sakai, H. Yoshinaga, H. Migamura, N. Kurigama and H. Ishikawa, *J. Alloys Compd.*, 180 (1992) 37
2. Y. Fukumoto, M. Miyamoto, M. Matsuoka and C. Iwakura, *Electrochimica Acta*, 40 (1995) 845
3. S. Yang, S. Han and J.Z. Song, Y. Li, *J. Rare Earth*, 29 (2011) 692
4. B.Z. Liu, A.M. Liu, Y.P. Fan, M.J. Hu and B.Q. Zhang, *Trans. Nonferr. Metals Soc. of China*, 22 (2012) 1730.
5. K. Komori, O. Yamamoto, Y. Toyoguchi, K. Suzuki, S. Yamaguchi, A. Tanaka and M. Ikoma, US5512385 (1996)
6. H. Ye, H. Zhang, W.Q. Wu and T.S. Huang, *J. Alloys Compd.*, 312 (2000) 68
7. Y.H. Zhang, M.Y. Chen, X.L. Wang, G.Q. Wang, X.P. Dong and Y. Qi, *Electrochim. Acta*, 49 (2004) 1161
8. S.Q. Yang, S.M. Han, Y. Li, S.X. Yang and L. Hu, *Mater. Sci. and Eng. B*, 176 (2010) 231
9. Y.P. Fan, B.Z. Liu, B.Q. Zhang, L.Q. Ji, Y.G. Wang and Z. Zhang, *Mater. Chem. Phys.*, (In press)
10. B.Z. Liu, M.J. Hu, Y.P. Fan, L.Q. Ji, X.L. Zhu and A.M. Li, *Electrochim. Acta*, 69 (2012) 384
11. B.Z. Liu, M.J. Hu, L.Q. Ji, Y.P. Fan, Y.G. Wang, Z. Zhang and A.M. Li, *J. Alloys Compd.*, 516 (2012) 53
12. X.Y. Peng, B.Z. Liu, Y.P. Fan, Li.Q. Ji, B.Q. Zhang and Z. Zhang, *Int. J. Electrochem. Sci.*, 8 (2013) 2262
13. K.Y. Shu, S.K. Zhang, Y.Q. Lei, G.L. Lü and Q.D. Wang, *Int. J. Hydrogen Energy*, 28 (2003) 1101
14. Y. Zhao, Y. Zhang, G. Wang, X. Dong, S. Guo and X. Wang, *J. Alloys Compd.*, 388 (2005) 284
15. W. Choi, K. Yamataka, S. Zhang and H. Inoue, C. Iwakura, *J. Electrochem. Soc.*, 146 (1999) 46
16. C. Iwakura, W. Choi, S. Zhang, H. Inoue, *Electrochim. Acta*, 44 (1999) 1677
17. D. Yan, G. Sandrock and S. Suda, *J. Alloys Compd.*, 216 (1994) 237
18. H. Yan, F. Kong, W. Xiong, B. Li, J. Li and L. Wang, *Int. J. Hydrogen Energy*, 35 (2010) 5687
19. S.R. Ovshinsky, M.A. Fetcenko and J. Ross, *Science*, 260 (1993) 176.
20. H.G. Pan, J.X. Ma, C.S. Wang, S.A. Chen, X.H. Wang and Q.D. Wang, *J. Alloys Compd.*, 293-295 (1999) 648
21. P. Notten and P. Hokkeling, *J. Electrochem. Soc.*, 138 (1991) 1877
22. H. Ye, Y.X. Huang, J.X. Chen and H. Zhang, *J. Power Sources*, 103 (2002) 293

23. Y.F. Liu, H.G. Pan, M. X. Gao, R. Li, X. Z. Sun and Y. Q. Lei, *J. Alloys Compd.*, 388 (2005) 109
24. B.V. Ratnakumar, C. Witham, R.C. Bowman Jr., A. Hightower and B. Fultz, *J. Electrochem. Soc.*, 143 (1996) 2578
25. C. Khaldi, H. Mathlouthi, J. Lamloumi and A. Percheron-Guegan, *J. Alloys Compd.*, 360 (2003) 266
26. D. Chartouni, F. Meli, A. Zuttel, K. Gross and L. Schlapbach, *J. Alloys Compd.*, 241 (1996) 160
27. B.Z. Liu, G.X. Fan, Y.C. Wang, G.F. Mi, Y.M. Wu and L.M. Wang, *Int. J. Hydrogen Energy*, 33 (2008) 5801
28. P. Li, X.L. Wang, Y.H. Zhang, R. Li, J.M. Wu and X.H. Qu, *J. Alloys Compd.*, 353 (2003) 278